



ELSEVIER

Computers and Geotechnics 27 (2000) 79–100

COMPUTERS  
AND  
GEOTECHNICS

www.elsevier.com/locate/compgeo

# Computation of individual contributions of two compression waves in vibration of water-saturated soils

Jun Yang\*, Tadanobu Sato

*Section of Dynamics of Foundation structure, Disaster Prevention Research Institute, Kyoto University, Gokasho, Uji, Kyoto 611-0011, Japan*

Received 7 January 2000; received in revised form 2 May 2000; accepted 3 May 2000

---

## Abstract

Water-saturated porous materials can sustain two types of compression waves, of which the second type is highly attenuated. Although the characteristics of independent waves of these two types are known, the knowledge of their individual contributions in dynamic response of saturated soils is limited. In this paper, a study is presented for a boundary value problem to quantitatively compute the individual contributions of these two waves. The problem corresponds to a water-saturated soil column subjected to steady-state vertical vibration at the base. The two-phase behaviour of soil is represented by the complete Biot's theory, which accounts for both viscous and mass couplings as well as the compressibility of constituents. A separation analysis procedure is presented which makes it possible to rigorously derive various responses such as displacement, total stress, pore pressure and relative fluid flow velocity in terms of the individual parts due respectively to the two compression waves. Numerical results are given to illustrate the behaviour of individual parts as affected by viscous coupling, mass coupling as well as loading frequency. © 2000 Elsevier Science Ltd. All rights reserved.

*Keywords:* Saturated soil; Dynamic response; Compression wave; Vibration

---

## 1. Introduction

It is known that soil can be more appropriately regarded as a two-phase porous continuum which is composed of a soil skeleton and pore water. Ocean sediments

---

\* Corresponding author. Tel.: +81-774-38-4068; fax: +81-774-38-4070.

*E-mail address:* yang@catfish.dpri.kyoto-u.ac.jp (J. Yang).

and rocks may also be seen as materials of this category. The dynamics of water-saturated porous materials is therefore of considerable interest in geotechnics, offshore engineering and seismology. The behaviour of water-saturated porous material differs considerably from that of single phase solids due principally to the presence of pore water. One fundamental difference is the existence of a second type of compression wave in saturated media in addition to the compression wave of the first type and the shear wave which are similar to the corresponding ones in ordinary elastic theory for solids [1,2]. The second type of compression wave is a true propagating wave only in high frequency range while it is associated with a diffusion type process at low frequency due to viscous coupling between solid and fluid phases. The motion of the solid skeleton and pore fluid are nearly in phase during the propagation of the first compression wave, the attenuation of which by viscous damping is relatively small. On the other hand, the compression wave of the second kind results from the out-of-phase movements of the solid skeleton and pore fluid, and is highly attenuated. Figs. 1 and 2 show the computed velocity and attenuation of these two types of compression waves in a typical sand and a normally consolidated clay as a function of frequency. Here  $f_c$  denotes the characteristic frequency of porous soils, depending on the porosity, permeability and fluid viscosity [1], while  $Q$  is quality factor. As can be seen, the attenuation of the second compression wave is several orders higher than that of the first one at low frequencies which results in difficulty in detection. On the other hand, in the high frequency range the velocity of the second compression wave is close to that of shear wave which makes it hard to distinguish them also [3]. The first experimental observation of the second compression wave was reported by Plona [4] in artificial porous materials. More recently, this type wave was successfully measured in granular soils by using a pulse transmission system combined with a conventional triaxial testing system [5].

Due to its high damping characteristics, it is natural to think that in the dynamic response of a saturated porous material the contribution from the second compression wave is much smaller than that from the first one and only the wave of the first type needs to be considered. However, this intuitive judgement has not yet been fully clarified in a quantitative sense because most problems corresponding to dynamic excitations applied to saturated porous materials (e.g. [6–10]) have been solved in an overall sense (i.e. the individual contributions from the two compression waves have not been explicitly identified). Some interesting issues related to the individual contributions in dynamic response, such as how the individual parts perform in the response, what is the influence of the viscous and mass couplings on the individual contributions, and the frequency-dependent behaviour of the individual parts are not very clear.

On the other hand, it has been shown that the presence of the compression wave of the second type has an effect upon the reflection and absorption at any saturated porous solid boundary although it is highly attenuated, suggesting that its existence may not be entirely overlooked especially in high frequency range [11,12]. Recently, it has been shown that the viscous coupling in poroelastic material is strongly affected by the hydraulic conditions at the boundary [13], which can produce a significant influence on the generation of the second compression wave [14,15]. Therefore,

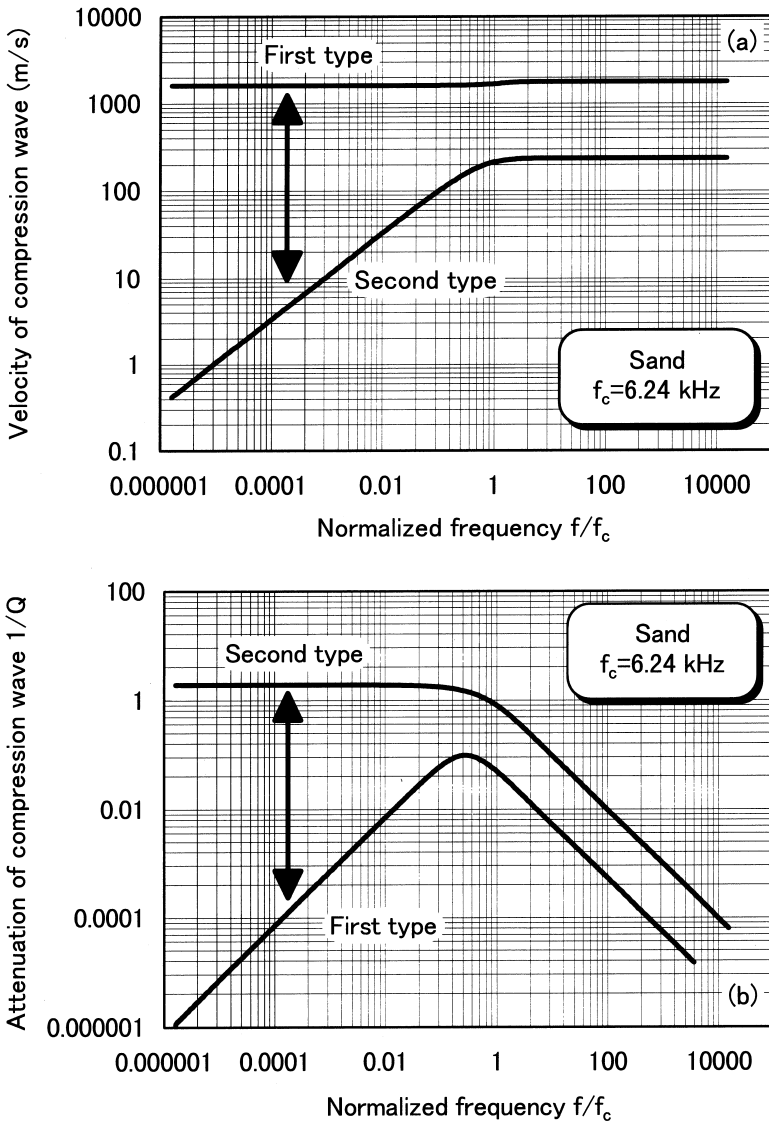


Fig. 1. Computed velocity and attenuation of two compression waves in a typical sand.

there remains a need and an interest to quantitatively examine the individual contributions of the two compression waves in dynamic response of saturated porous materials, which would provide a better understanding of dynamic behaviour of poroelastic materials. In particular, with the availability of laboratory measurement of the second compression wave in soil samples, the understanding presented in this study would be helpful in making use of its characteristics in determining some soil properties [3].

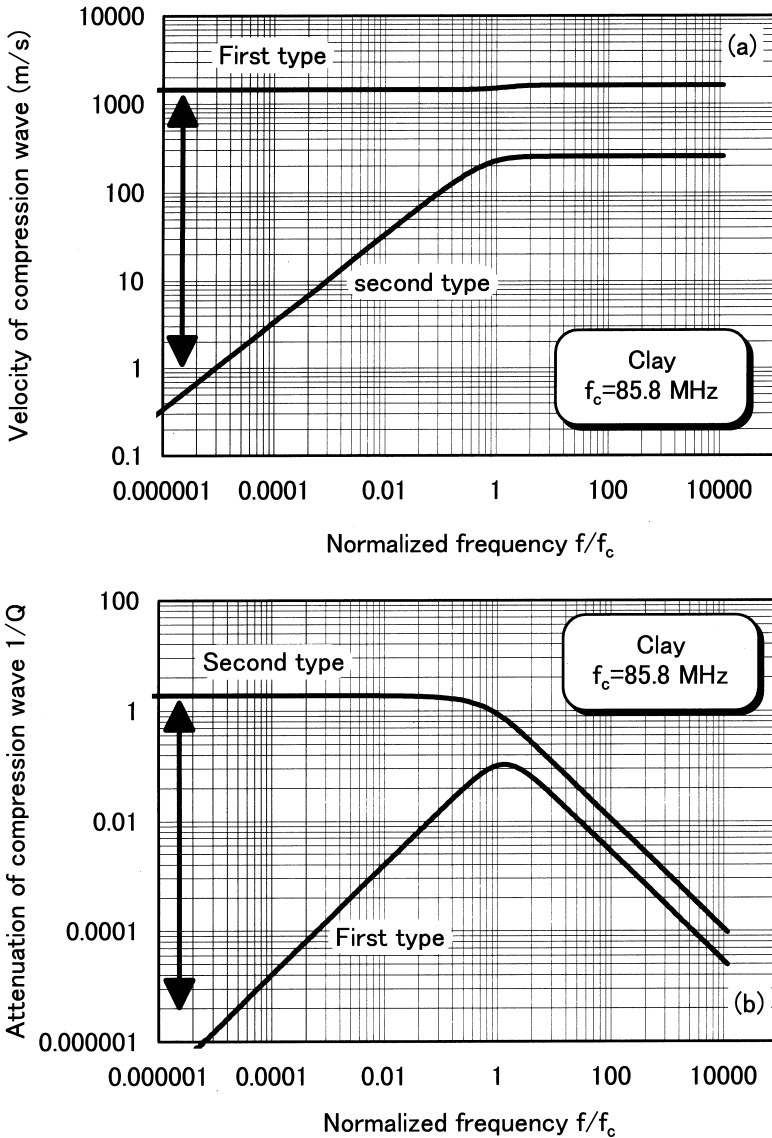


Fig. 2. Computed velocity and attenuation of two compression waves in a typical clay.

To this end, a problem corresponding to the response of a water-saturated soil column subjected to steady-state vertical base excitation is analyzed herein. The soil is modeled as a saturated two-phase material by using complete Biot's theory, which takes into account not only the compressibility of the soil grains, soil skeleton and pore water, but also the dissipation due to the fluid viscosity and the mass coupling between the two phases. A separation analysis procedure is presented, which makes

it possible to rigorously derive the responses of displacement, total stress and pore pressure in terms of the individual contributions of the two types of waves. Numerical results are presented to show the behaviour of individual parts as affected by viscous and mass couplings as well as loading frequency.

**2. Governing equations and separation analysis**

The physical model considered in this study is shown in Fig. 3. The steady-state displacement excitation is acting at the impermeable, rigid base ( $z=0$ ) of a water-saturated soil column, while the surface of the column ( $z=L$ ) is stress-free and free draining. This model may correspond to a soil layer subjected to vertical seismic action in the field or represent a shaking table case (in vertical direction) in the laboratory [16]. In the context of Biot’s theory, the governing equations for this one-dimensional problem can be written as [13]

$$(\lambda_c + 2\mu) \frac{\partial^2 u}{\partial z^2} + \alpha M \frac{\partial^2 w}{\partial z^2} = \rho \frac{\partial^2 u}{\partial t^2} + \rho_f \frac{\partial^2 w}{\partial t^2} \tag{1}$$

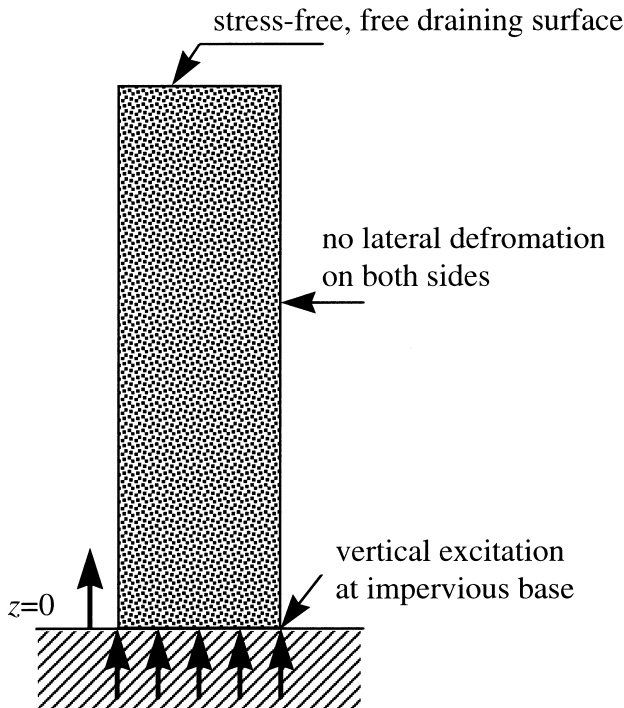


Fig. 3. A soil column subjected to vertical excitation at rigid base.

$$\alpha M \frac{\partial^2 u}{\partial z^2} + M \frac{\partial^2 w}{\partial z^2} = \rho_f \frac{\partial^2 u}{\partial t^2} + m \frac{\partial^2 w}{\partial t^2} + b \frac{\partial w}{\partial t} \quad (2)$$

where  $u$  and  $w$  are, respectively, displacements of solid skeleton and pore fluid with respect to the solid phase;  $\rho_s, \rho_f$  are mass densities of solid grains and fluid, respectively,  $\rho = (1 - n)\rho_s + n\rho_f$ ,  $n$  is porosity; the parameter  $m$  describes the mass coupling effect and depends on the density of fluid and the geometry of the pores and can be expressed as  $m = s\rho_f/n$ ,  $s$  is the experimentally determined parameter known as the structure factor [2,17]; the parameter  $b$  accounts for the viscous coupling due to the relative motion between the solid and fluid phases, which is defined as  $\eta/k$ ,  $\eta$  is the fluid viscosity and  $k$  is the permeability with the unit  $\text{m}^2$ . In the case of high frequency where the assumption of Poiseuille flow is not valid, the viscosity may depend upon frequency and pore structure in a complicated manner, as discussed in [2,18]. In most situations this is not the case of concerned.  $\lambda, \mu$  are the Lamé's constants,  $\lambda_c = \lambda + \alpha^2 M$ ,  $\alpha, M$  are the parameters accounting for the compressibility of the solid and fluid constituents, they can be given as

$$\alpha = 1 - \frac{K_b}{K_s} \quad M = \frac{K_s^2}{K_d - K_b} \quad K_d = K_s[1 + n(\frac{K_s}{K_f} - 1)] \quad (3)$$

in which  $K_s, K_f$  and  $K_b$  are the bulk moduli of solid grains, fluid and solid skeleton, respectively. For incompressible solid grains only,  $\alpha = 1$ , while for both grains and pore fluid incompressible,  $\alpha = 1$  and  $1/M = 0$ . The inclusion of the compressibility of constituents is one important feature of Biot's theory although it is usually simplified in soil mechanics as seen in [7].

It should be noted that  $k$  in our formulation is different from the permeability coefficient  $k'$  (m/s) that is used in soil mechanics and they are related by

$$k = k' \frac{\eta}{\rho_f g} \quad (4)$$

in which  $g$  is the gravitation acceleration at which the permeability is measured.

For the linear, coupled problem considered, to separate individual contributions from two types of compression waves one may directly break down the displacements as

$$u = u_1 + u_2 \quad w = w_1 + w_2 \quad (5)$$

and  $u_1, w_1, u_2, w_2$  satisfy the following relationships

$$u_1 = \delta_1 w_1 \quad u_2 = \delta_2 w_2 \quad (6)$$

where  $u_1, w_1$  are attributed to the first compression wave, while  $u_2, w_2$  are associated with the compression wave of the second type.

For steady-state vibration with circular frequency  $\omega$  ( $e^{i\omega t}$ ), substitution of the above equations into the governing equations yields

$$[K][L]\{w\} + ([M] - [C])[Ω]\{w\} = \{0\} \tag{7}$$

in which

$$\begin{aligned}
 [K] &= \begin{bmatrix} (\lambda_c + 2\mu)\delta_1 + \alpha M & (\lambda_c + 2\mu)\delta_2 + \alpha M \\ \alpha M\delta_1 + M & \alpha M\delta_2 + M \end{bmatrix} \\
 [M] &= \begin{bmatrix} \rho\delta_1 + \rho_f & \rho\delta_2 + \rho_f \\ \rho_f\delta_1 + m & \rho_f\delta_2 + m \end{bmatrix} \quad [C] = \begin{bmatrix} 0 & 0 \\ ib/\omega & ib/\omega \end{bmatrix} \quad [L] = \begin{bmatrix} \nabla^2 & 0 \\ 0 & \nabla^2 \end{bmatrix} \\
 [Ω] &= \begin{bmatrix} \omega^2 & 0 \\ 0 & \omega^2 \end{bmatrix} \{w\} = \begin{Bmatrix} w_1 \\ w_2 \end{Bmatrix}
 \end{aligned} \tag{8}$$

Eq. (7) can be de-coupled only if  $\delta_1$  and  $\delta_2$  satisfy the following equations

$$\begin{aligned}
 &[\rho_f(\lambda_c + 2\mu) - \rho\alpha M]\delta^2 + [(\lambda_c + 2\mu)(m - ib/\omega) - \rho M]\delta \\
 &+ [\alpha M(m - ib/\omega) - \rho_f M] = 0
 \end{aligned} \tag{9}$$

The boundary conditions for the model considered are as follows: displacement excitation with a frequency  $\omega$  and amplitude  $U_0$  is acting at the impermeable, rigid base while the surface of the column is stress-free and free draining, that is

$$z = 0 : \quad u = U_0 e^{i\omega t} \quad w = 0 \tag{10}$$

$$z = L : \quad p_f = 0 \quad \sigma = 0 \tag{11}$$

where  $p_f$  is pore pressure

By enforcing these boundary conditions, the displacements can be derived in terms of individual parts from the two compression waves as (for brevity the steady-state factor  $e^{i\omega t}$  is omitted)

$$\begin{cases} u = u_1 + u_2 \\ u_1 = U_0 \frac{\delta_1}{\delta_1 - \delta_2} \frac{\cos[k_1(L - z)]}{\cos(k_1 L)} \\ u_2 = -U_0 \frac{\delta_2}{\delta_1 - \delta_2} \frac{\cos[k_2(L - z)]}{\cos(k_2 L)} \end{cases} \tag{12}$$

$$\begin{cases} w = w_1 + w_2 \\ w_1 = U_0 \frac{1}{\delta_1 - \delta_2} \frac{\cos[k_1(L - z)]}{\cos(k_1 L)} \\ w_2 = -U_0 \frac{1}{\delta_1 - \delta_2} \frac{\cos[k_2(L - z)]}{\cos(k_2 L)} \end{cases} \tag{13}$$

where  $k_1, k_2$  are complex wave numbers of the first and second compression waves, respectively, they can be given as

$$k_1^2 = \frac{(K_{12}M_{21} - K_{22}M_{11} - iK_{12}b/\omega)\omega^2}{K_{12}K_{21} - K_{11}K_{22}} \quad (14)$$

$$k_2^2 = \frac{(K_{11}M_{22} - K_{21}M_{12} - iK_{11}b/\omega)\omega^2}{K_{11}K_{22} - K_{21}K_{12}} \quad (15)$$

in which  $K_{ij}$ ,  $M_{ij}$  are corresponding elements of  $[K]$  and  $[M]$ ,  $i = \sqrt{-1}$ .

Given the following constitutive equations

$$\sigma_{ij} = \lambda u_{i,i} \delta_{ij} + \mu(u_{i,j} + u_{j,i}) - \alpha \delta_{ij} p_f \quad (16)$$

$$p_f = -M w_{i,i} - \alpha M u_{i,i} \quad (17)$$

where  $\sigma_{ij}$  is the total stress of the bulk material,  $\delta_{ij}$  is Kronecker delta, the stress and pore pressure can be obtained in terms of the contributions from the first ( $\sigma_1$  and  $p_{f1}$ ) and second compression waves ( $\sigma_2$  and  $p_{f2}$ ) as

$$\begin{cases} p_f = p_{f1} + p_{f2} \\ p_{f1} = -U_0(M + \alpha M \delta_1) \frac{k_1}{\delta_1 - \delta_2} \frac{\sin[k_1(L - z)]}{\cos(k_1 L)} \\ p_{f2} = U_0(M + \alpha M \delta_2) \frac{k_2}{\delta_1 - \delta_2} \frac{\sin[k_2(L - z)]}{\cos(k_2 L)} \end{cases} \quad (18)$$

$$\begin{cases} \sigma = \sigma_1 + \sigma_2 \\ \sigma_1 = U_0[(\lambda_c + 2\mu)\delta_1 + \alpha M] \frac{k_1}{\delta_1 - \delta_2} \frac{\sin[k_1(L - z)]}{\cos(k_1 L)} \\ \sigma_2 = -U_0[(\lambda_c + 2\mu)\delta_2 + \alpha M] \frac{k_2}{\delta_1 - \delta_2} \frac{\sin[k_2(L - z)]}{\cos(k_2 L)} \end{cases} \quad (19)$$

As for the relative fluid flow velocity, which reflects the important viscous damping in saturated porous material [13], it can be directly obtained by multiplying the fluid displacement by  $i\omega$ .

### 3. Behaviour of individual contributions of two compression waves

In this section, numerical computation based on the preceding solutions is presented to illustrate the characteristics of the individual contributions from the two compression waves. The properties of a clean coarse sand, as listed in Table 1, are used in the computation.

Table 1  
Soil properties used in computation

Quantity	Notation	Value
Bulk modulus of solid skeleton	$K_b$	86.7 MPa
Bulk modulus of solid grains	$K_s$	36 GPa
Bulk modulus of water	$K_w$	2 GPa
Lame constant of solid skeleton	$\mu$	40 MPa
Permeability	$k$	$10^{-10} \text{ m}^2$
Fluid viscosity	$\eta$	$10^{-3} \text{ N s/m}^2$
Density of grains	$\rho_s$	2650 kg/m <sup>3</sup>
Porosity	$n$	0.4
Pore structure factor	$s$	1

### 3.1. Response of relative flow velocity

As is well known, a key feature of saturated porous material is that it takes on a viscous character due to the motion of pore fluid with respect of the solid matrix. Therefore, the behaviour of fluid flow is of interest and worth mentioning. Fig. 4 shows the distribution of the relative flow velocity in the column for a natural frequency  $f = 5 \text{ Hz}$ . The length of the column is taken as 15 m. The real and imaginary components of the relative flow velocity are presented in Fig. 4(a) and (b), respectively, in each of them P-1 and P-2 denote the contributions from the first and second compression waves, and P-t denotes the sum of the net individual contributions. The flow velocity is normalized here by  $\omega U_0$ . Obviously, the individual contributions from the two waves are quite different. It is seen that while the real and imaginary parts of the first compression wave are practically constant in the layer, the components due to the second compression wave vary significantly, especially within a range near the bottom boundary where the exciting source is acting. In this range (about  $0.2L$  upward from the bottom), the curve representing the sum of the contributions takes the trend of the curve for the second compression wave. The range is referred to herein as the “influence range” from this wave, within such a range the contribution from the second compression wave is comparable to that from the first one. Outside the range, the contribution from this wave is negligible due to its high attenuation. It is also noted that the individual contributions from these two waves are exactly equal but opposite in sign at the bottom. This is understandable, since the bottom boundary is impervious, the solid and fluid phases have to move together so as to prevent the relative fluid motion.

It is known that the permeability is an important property which characterizes the porous media and reflects the viscous coupling between the two phases. The importance of viscous coupling has recently been discussed for reflection and transmission of waves at a saturated porous boundary [13]. Its influence on the fluid flow, especially on the individual performance, is interesting. Fig. 5(a) and (b) show the real and imaginary components of flow velocity for a different permeability  $k = 10^{-9} \text{ m}^2$  for the same frequency. Besides such similar features described earlier can be observed from Fig. 5 itself, by comparing Figs. 4 and 5, it is found that the permeability is

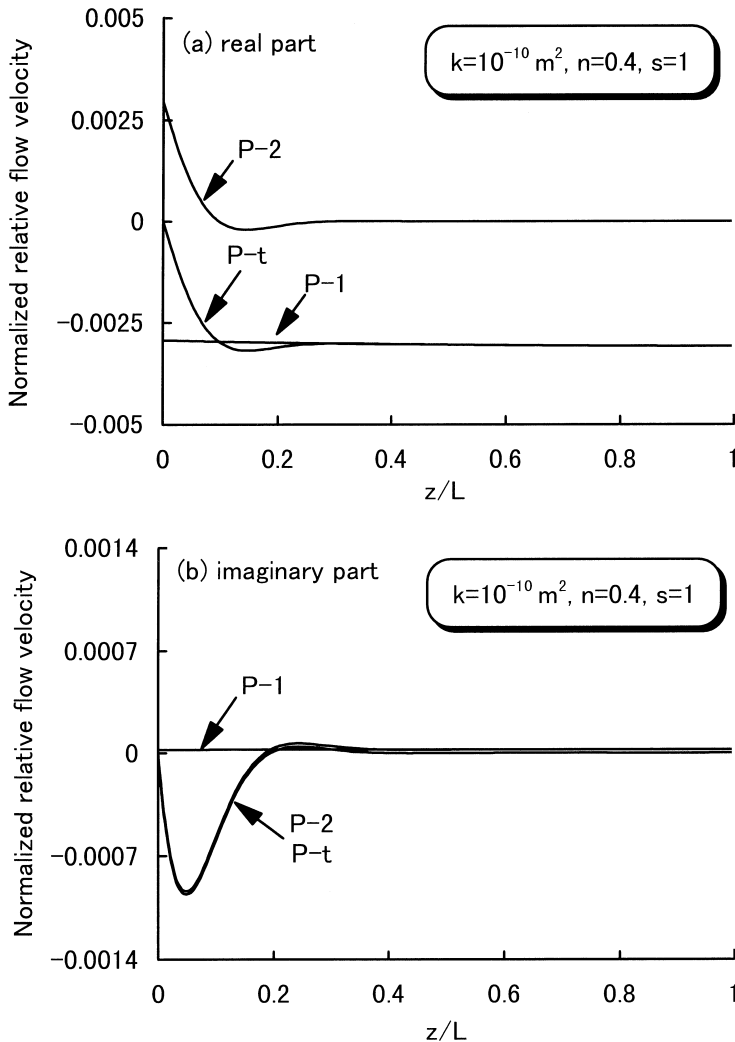


Fig. 4. Relative flow velocity in terms of individual contributions from two compression waves as a function of location ( $k = 10^{-10} \text{ m}^2$ ).

important for both the individual contributions. The magnitude increases almost by an order when the permeability increases from  $k = 10^{-10} \text{ m}^2$  to  $k = 10^{-9} \text{ m}^2$ . This finding is certainly reasonable from an intuitive point of view, since the lower the permeability, the resistance between the solid and fluid is larger and subsequently the relative fluid flow is small. Moreover, an interesting picture is noticed that the permeability also produces a significant influence on the influence range of the second compression wave. It is found that the influence range extends from  $0.2L$  to  $0.6L$  with increasing permeability. The reason is that the influence of permeability on the damping of the second wave results in the extension of its attenuation distance.

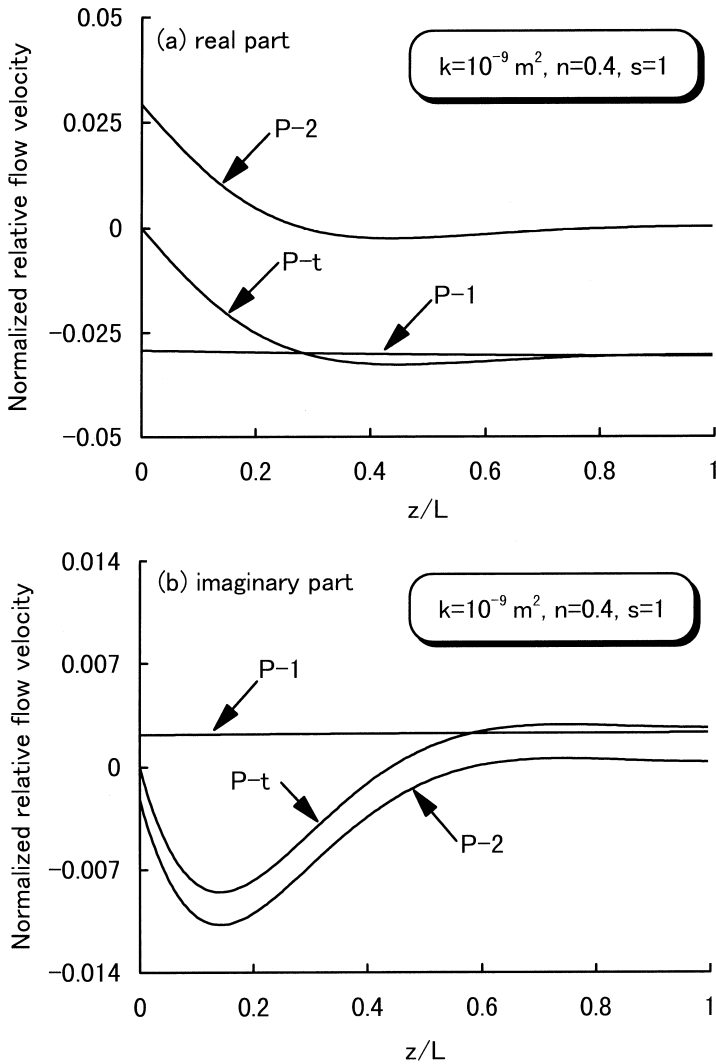


Fig. 5. Relative flow velocity in terms of individual contributions from two compression waves as a function of location ( $k = 10^{-9} \text{ m}^2$ ).

Porosity and pore structure factor are another two properties of saturated porous material which reflect the mass coupling effect arising from the fact that, for a typical porous system, the motion of the pore fluid is not the uniform and in general does not take place in the direction of the macroscopic pressure gradient. For uniform, cylindrical pores with axes parallel to the gradient, the pore structure factor  $s$  is equal to 1; whereas for a random system of pores with all possible orientations,  $s$  may take the value of 3 [17]. To examine the effects of mass coupling on the

individual parts, the results for relative flow velocity are computed for a different porosity  $n=0.6$  and a pore structure factor  $s=3$ , as shown in Figs. 6 and 7. The permeability is taken as  $k = 10^{-10} \text{ m}^2$ . Compared to the effects of viscous coupling, the influence of porosity and pore structure factor is in general not appreciable.

3.2. Response of solid displacement

The distribution of displacement of the solid skeleton is plotted in Fig. 8 for the same frequency. The displacement is normalized with the base displacement  $U_0$  and

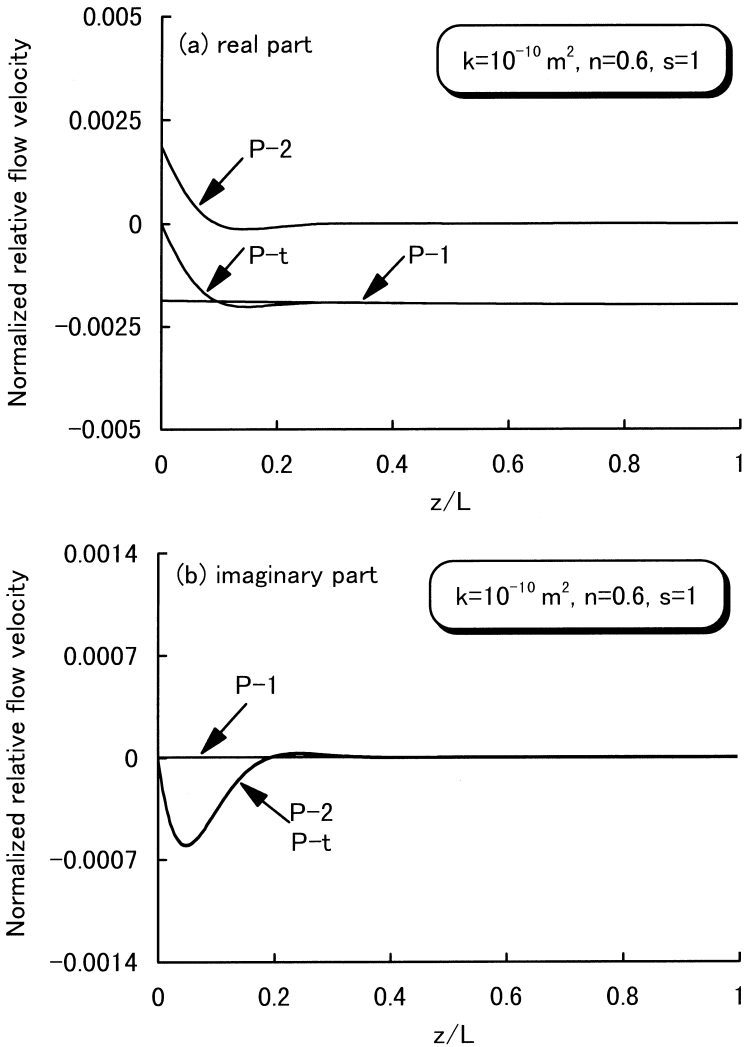


Fig. 6. Relative flow velocity in terms of individual contributions as a function of location ( $n=0.6$ ).

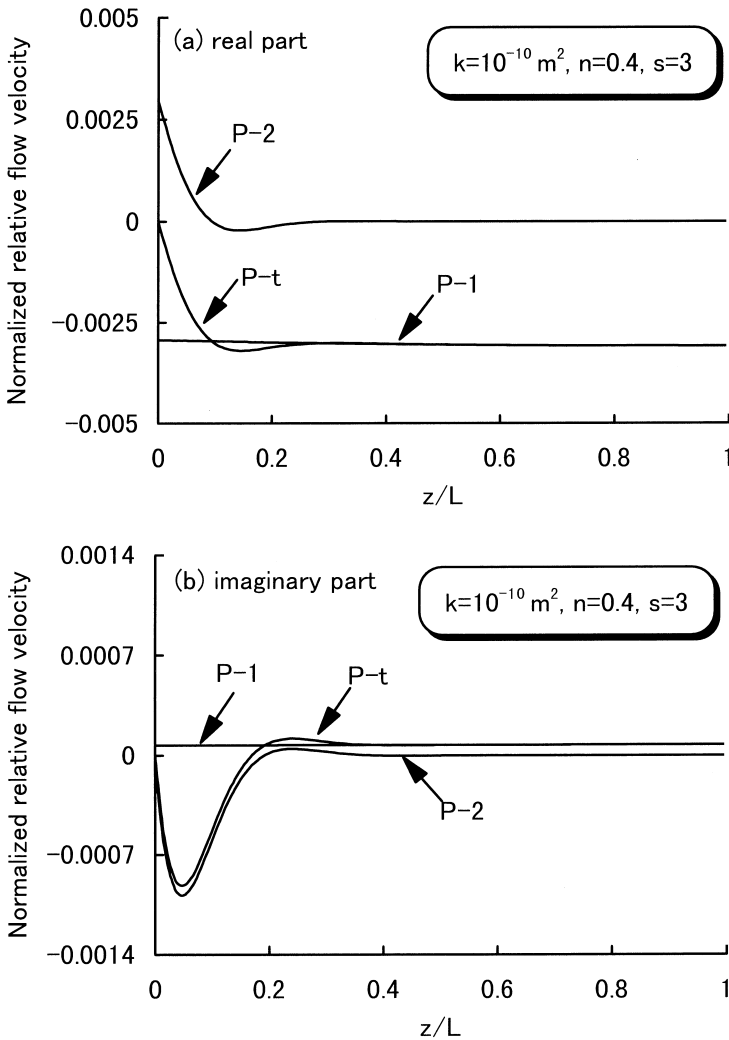


Fig. 7. Relative flow velocity in terms of individual contributions as a function of location ( $s=3$ ).

the permeability is taken as  $10^{-10} \text{ m}^2$ . As can be seen, the dominant component of the solid displacement is the real one from the first compression wave. In other words, the contribution to the solid displacement comes mainly from this wave, whose attenuation is very small, while the contribution of the second wave is negligible. This result is reasonable if one considers the great difference of  $\delta_1$  and  $\delta_2$  in magnitude. As far as the second compression wave is concerned, it is observed that its imaginary component changes considerably within the region near the bottom. Similar behaviour can be found in Fig. 9 in which the results are shown for the

permeability  $k = 10^{-9} \text{ m}^2$ . The comparison of Figs. 8 and 9 shows that the influence of permeability is notable only on the imaginary components, which are obviously increased. Similarly, the influence range of the second compression wave also extends as the permeability increases.

As for the influence of porosity and pore structure factor, it is very slight on the solid displacement, even smaller than that for relative flow velocity. For brevity, the related results are not presented here.

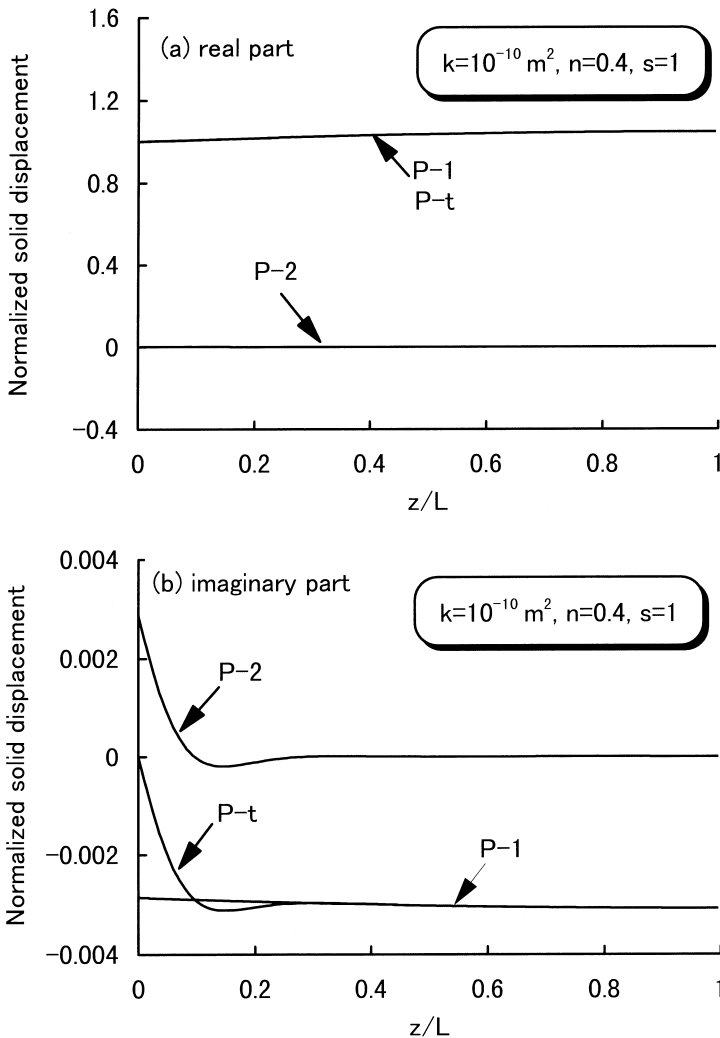


Fig. 8. Solid displacement in terms of individual contributions from two compression waves as a function of location ( $k = 10^{-10} \text{ m}^2$ ).

3.3. Response of pore pressure

The distribution of pore pressure in the column for  $f=5$  Hz and  $k=10^{-10}$  m<sup>2</sup> is shown in Fig. 10. The pore pressure is normalized by  $\bar{p}_f = p_f/\sigma_0$ ,  $\sigma_0 = U_0(\lambda + 2\mu)/L$ . The results for the permeability  $k=10^{-9}$  m<sup>2</sup> are plotted in Fig. 11 to show the effect of viscous coupling. As can be seen, the major contribution to the pore pressure comes from the first compression wave. The pore pressure varies from the maximum value at the bottom to the zero at the surface. This behaviour is

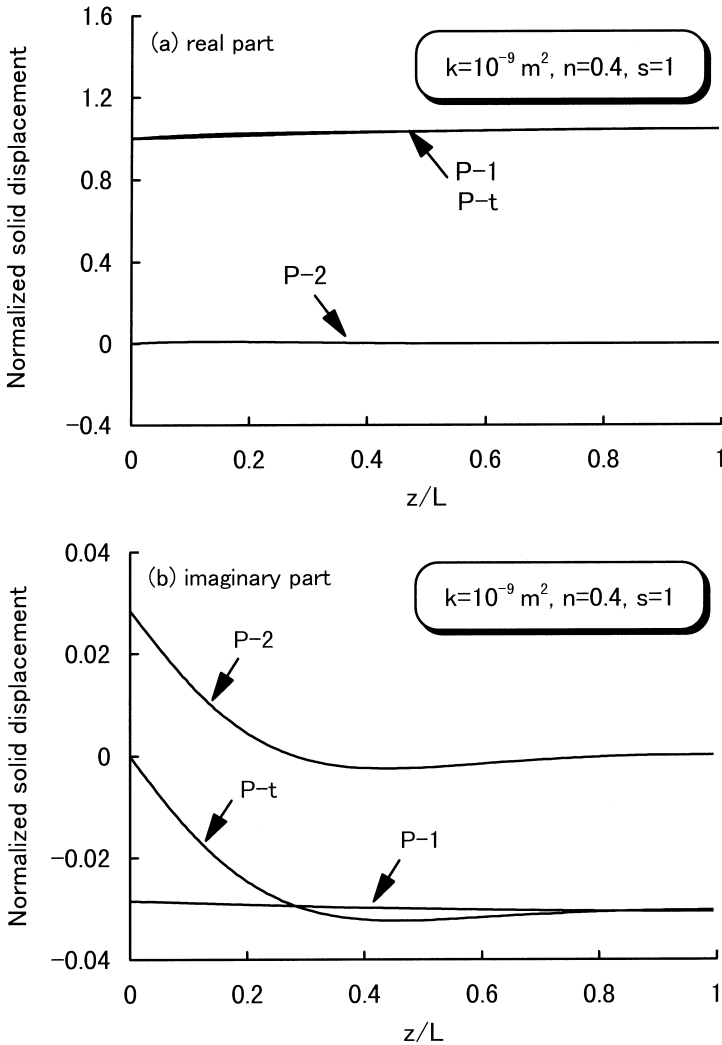


Fig. 9. Solid displacement in terms of individual contributions from two compression waves as a function of location ( $k=10^{-9}$  m<sup>2</sup>).

understandable because the column surface is free draining, leading to the vanishing of pore pressure at such boundary and an establishment of pore pressure gradient within the column. It is also observed that the imaginary part due to the second type of compression wave drops rapidly near the bottom boundary and the effect of permeability is significant. The increasing permeability produces an obvious increment in the influence range of the second wave. Similarly, small effects of porosity and pore structure factor are observed on pore pressure distribution.

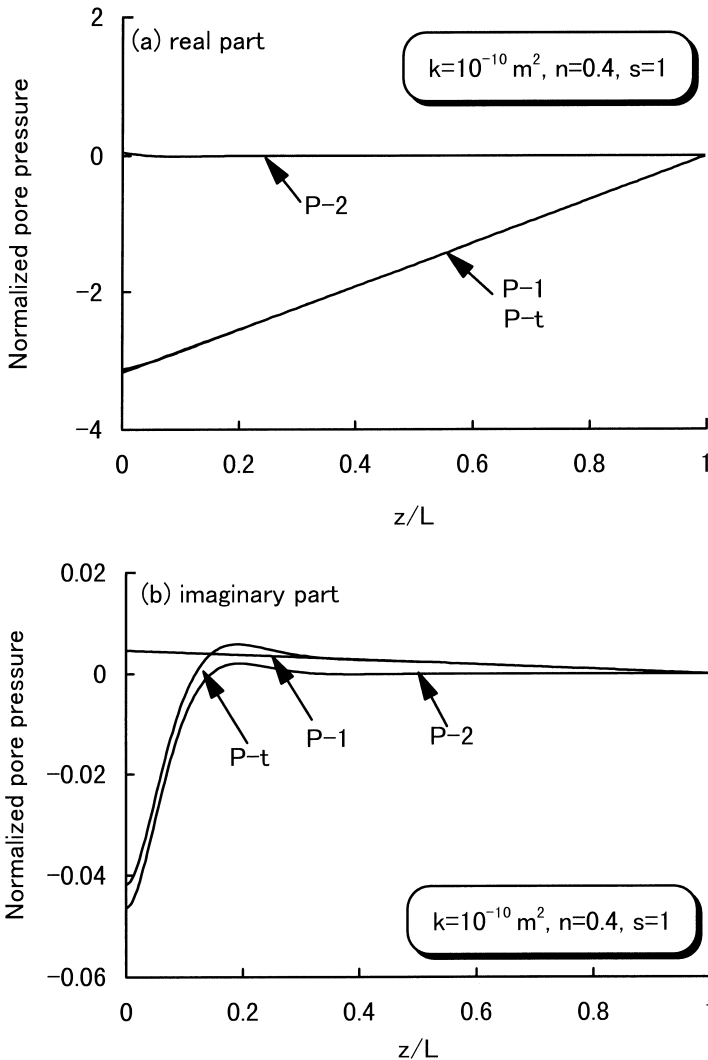


Fig. 10. Pore pressure in terms of individual contributions from two compression waves as a function of location ( $k=10^{-10} \text{ m}^2$ ).

3.4. Frequency dependent response

The preceding results are obtained for a specified frequency  $f=5$  Hz. Due to the inclusion of fluid viscosity in the present study, the waves in saturated soil are dispersive, namely, frequency dependent. The frequency-dependent behaviour of individual parts in various responses needs identification. The solid displacement due to the first and second compression waves are shown in Fig. 12(a) and (b), respectively, as a function of frequency. The responses of normalized pore pressure and relative

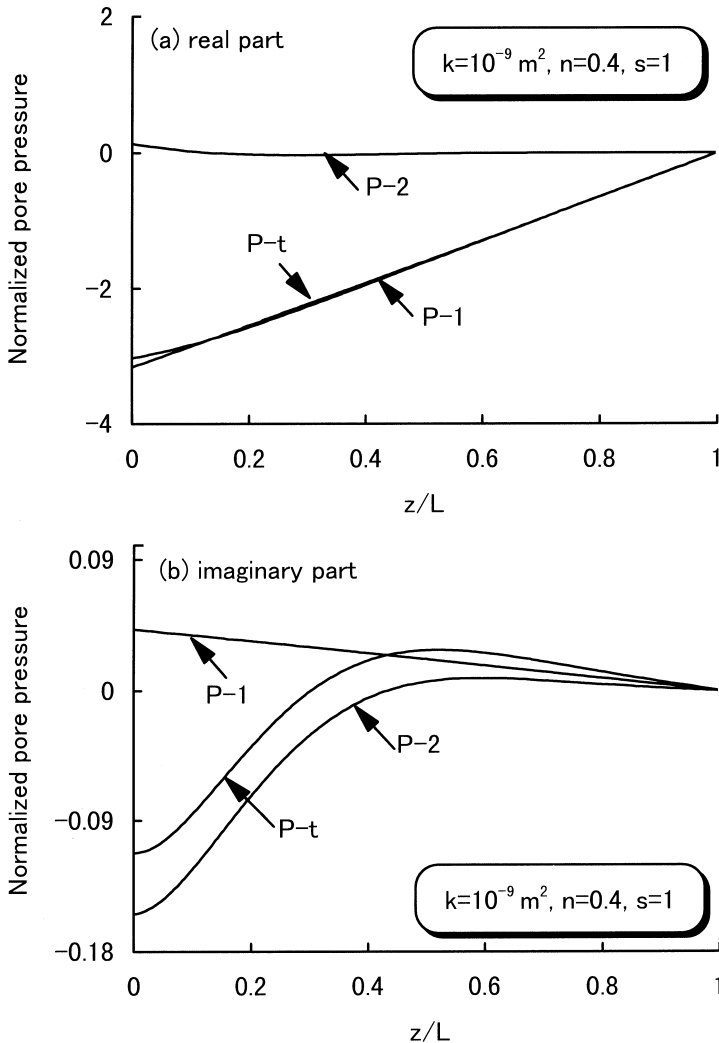


Fig. 11. Pore pressure in terms of individual contributions from two compression waves as a function of location ( $k=10^{-9} \text{ m}^2$ ).

flow velocity are shown in Figs. 13 and 14, respectively. In each figure, two cases of permeability are included to simultaneously show the influence of viscous coupling. All these responses are located at the position of  $z = L/10$ . In the computation the porosity is taken as 0.4 and the pore structure factor is 1. The frequency is normalized here as  $\bar{\omega} = 2\omega L/\pi V_0$ , where  $V_0 = \sqrt{(\lambda_c + 2\mu)/\rho}$  is the velocity of the first compression wave at low frequency limit [13]. All the responses due to the second compression wave for the case of  $k = 10^{-10} \text{ m}^2$  are multiplied by a factor of 10 to give a better view.

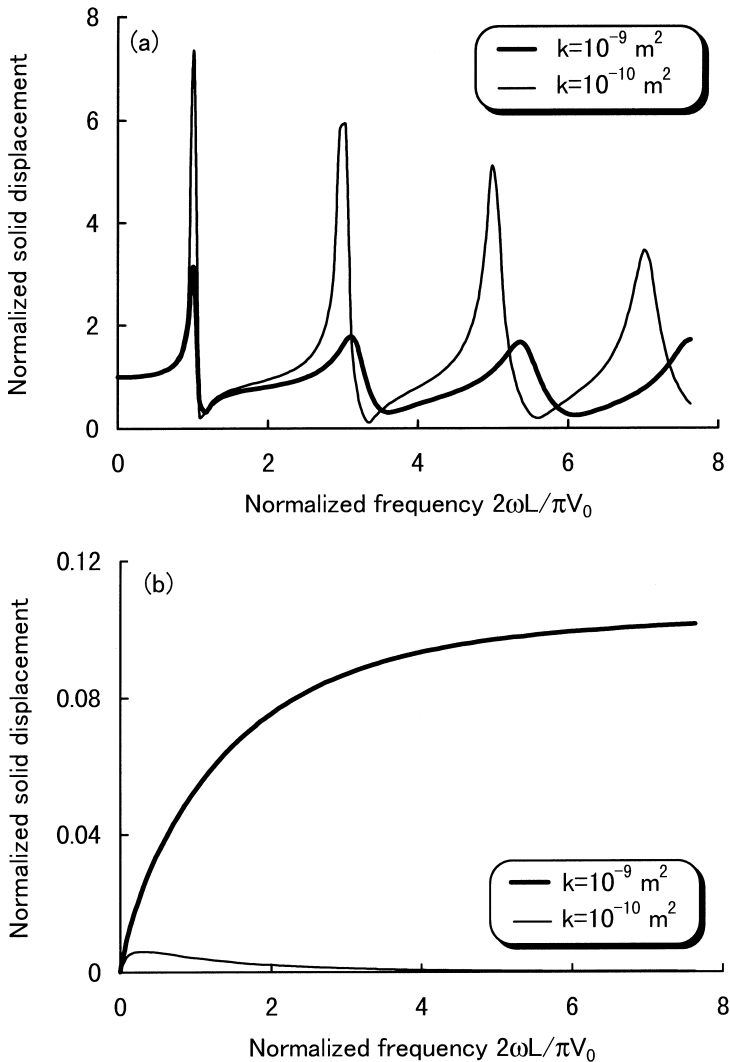


Fig. 12. Solid displacement at a specified location as a function of frequency; (a) contribution of the first compression wave; (b) contribution of the second compression wave.

Quite a different behaviour in responses is noticed for the two types of waves. The responses due to the first compression wave peak when the dimensionless frequency is equal to about  $(2j - 1)$  where  $j$  is a positive integer. However, the responses attributed to the second wave do not exhibit such a common frequency-dependent performance. It may be considered that this feature is associated with the characteristic of this wave, that is, the second compression wave is in fact a diffusion-type process, not a true propagating wave at low frequencies because of the viscous damping.

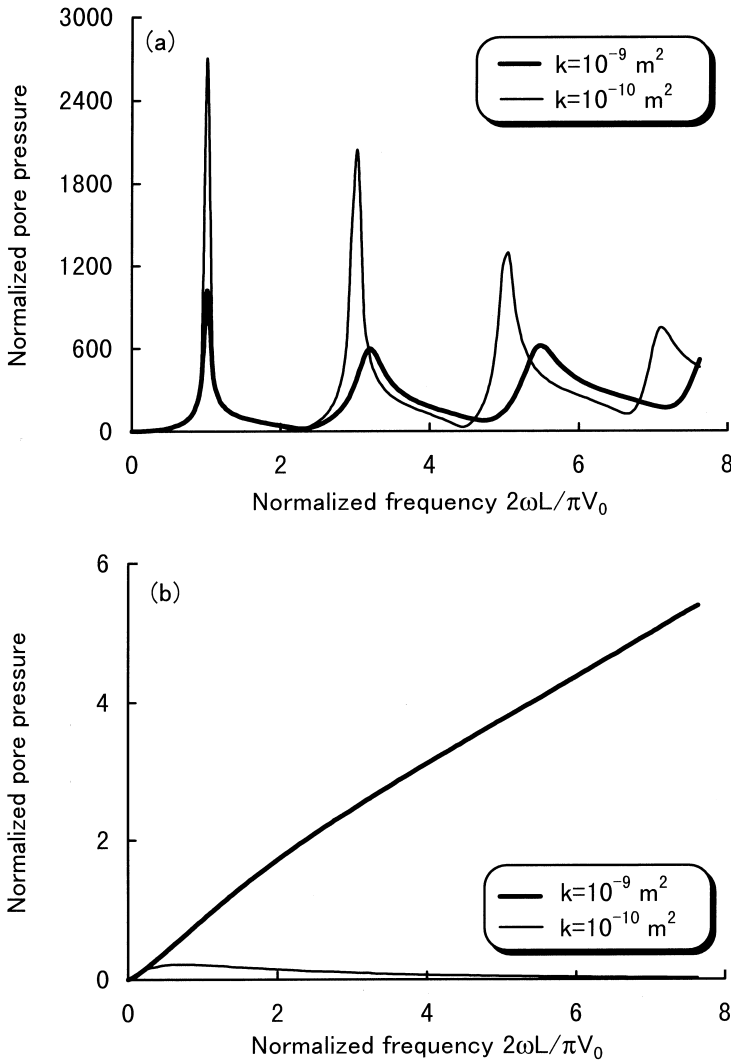


Fig. 13. Pore pressure at a specified location as a function of frequency; (a) contribution of the first compression wave; (b) contribution of the second compression wave.

On the other hand, it is observed that the effect of permeability is significant on the frequency-dependent responses. As shown in Figs. 12(a) and 13(a), the increase of permeability causes a sizable decrease of the peak values and a slight increase of the resonant frequencies for solid displacement and pore pressure responses. The frequency-dependent behaviour due to the first compression wave is almost same with the overall response behaviour (i.e. no separation [16]), in other words, the first compression wave dominates in such performance. On the other hand, for the flow velocity response, the increase of permeability results in the peak values increasing.

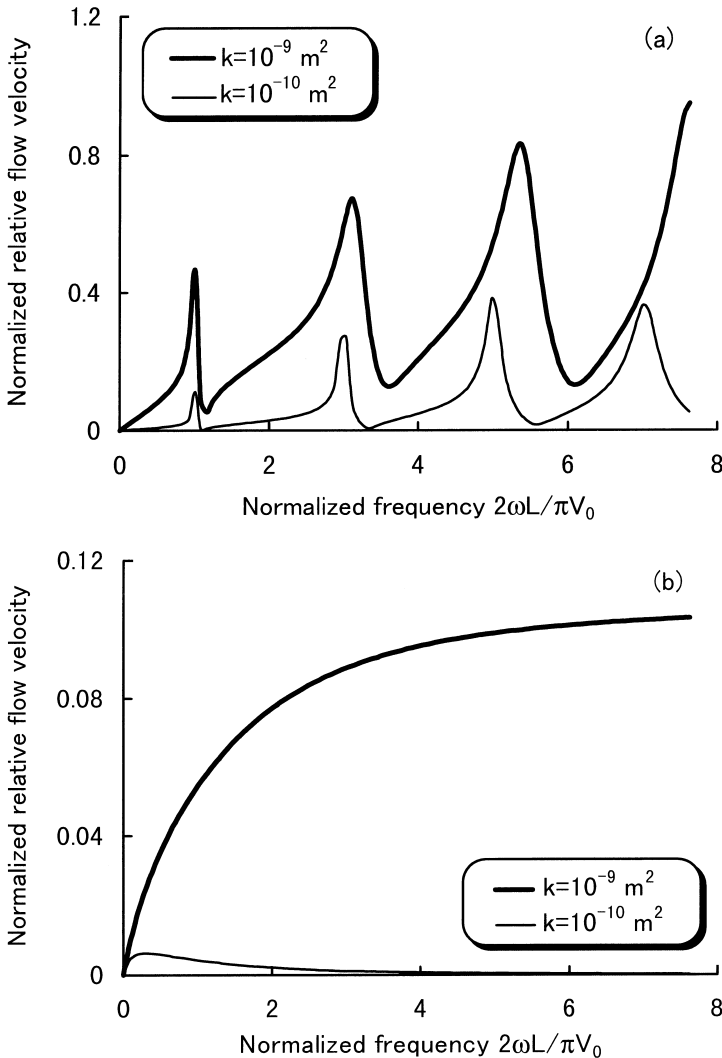


Fig. 14. Relative flow velocity at a specified location as a function of frequency; (a) contribution of the first compression wave; (b) contribution of the second compression wave.

In addition, it is noted that, in either case of permeability, the peak values of flow velocity increase with the frequency. This implies that, in a general sense, there is little relative fluid motion in low frequency range or at high viscous coupling, while it becomes larger at high frequencies or low viscous coupling [13].

#### **4. Concluding remarks**

The individual contributions from two types of compression waves in the vibration of a water-saturated soil column is examined quantitatively. Analytical solutions for various responses are rigorously derived in terms of individual contributions by means of a separation procedure. Numerical results indicate that the contribution of the first compression wave is dominant in the responses of solid displacement and pore pressure, while the contribution from the second compression wave is very small. As for the fluid flow velocity, the contribution from the second compression wave is comparable to that of the wave of the first kind within a defined influence range. In general, the effect of viscous coupling/permeability on the responses due to the second compression wave is significant, especially on the influence range, which obviously increases with increasing permeability. Compared to the viscous coupling effect, the influence of mass coupling is however very small on both individual parts. As far as the frequency-dependent behaviour is concerned, the response due to the second compression wave is quite different from that due to compression wave of the first one. The observed overall responses of solid displacement and pore pressure are almost due to the contribution from the first compression wave.

Finally, it should be mentioned that, although the contribution from the second compression wave is in general very small compared to its counterpart, both the rigorous solutions and numerical results presented in this paper show that all the responses consist of two individual parts due respectively to the two compression waves, convincingly indicating that the common understanding in geotechnical engineering community [19] is not accurate that among the two compression waves one propagates in the fluid and the other in the solid.

#### **Acknowledgements**

The financial aid received from the Ministry of Education and Science, Japan, via the program of Center of Excellence (COE), and the aid from Japan Society of Civil Engineers via STA project are greatly acknowledged. Thanks also go to the referees for their careful reviews and suggestions.

#### **References**

- [1] Biot MA. Theory of propagation of elastic waves in a fluid saturated porous solid. *Journal of Acoustical Society of America* 1956;28:168–91.
- [2] Biot MA. Mechanics of deformation and acoustic propagation in porous media. *Journal of Applied Physics* 1962;33:1482–98.

- [3] Yang J, Sato T. On the velocity and damping of nearly-saturated soils. In: Proceedings of the 33rd Japan National Conference on Geotechnical Engineering, Yamaguchi, 1998.
- [4] Plona TJ. Observation of a second bulk compressional wave in a porous medium at ultrasonic frequencies. *Applied Physics Letters* 1980;36:259–61.
- [5] Nakagawa K, Soga K, Mitchell JK. Observation of Biot compressional wave of the second kind in granular soils. *Geotechnique* 1997;47:133–47.
- [6] Ghaboussi J, Wilson EL. Variational formulation of dynamics of fluid-saturated porous elastic solids. *Journal of Engineering Mechanics, ASCE* 1972;94:7–63.
- [7] Zienkiewicz OC, Chang CT, Bettles P. Drained, undrained, consolidating and dynamic behaviour assumptions in soils. *Geotechnique* 1980;30:385–95.
- [8] Mei CC, Foda MA. Wave-induced responses in a fluid-filled poroelastic solid with a free surface: a boundary layer theory. *Geophysics Journal of Royal Astronomical Society* 1981;66:597–631.
- [9] Vardoulakis I, Beskos DE. Dynamic behaviour of nearly saturated porous media. *Mechanics of Materials* 1986;5:87–108.
- [10] Bardet JP. A viscoelastic model for the dynamic behavior of saturated poroelastic soils. *Journal of Applied Mechanics, ASME* 1992;59:128–35.
- [11] Geertsma J, Smit D. Some aspect of elastic wave propagation in a fluid-saturated porous solid. *Geophysics* 1961;26:169–81.
- [12] Wu K, Xue Q, Adler L. Reflection and transmission of elastic waves from a fluid-saturated porous solid boundary. *Journal of Acoustical Society of America* 1990;87:2349–58.
- [13] Yang J, Sato T. Influence of viscous coupling on seismic reflection and transmission in saturated porous media. *Bulletin of Seismological Society of America* 1998;88:1289–99.
- [14] Yang J. Importance of flow condition on seismic waves at a saturated porous solid boundary. *Journal of Sound and Vibration* 1999;221:391–413.
- [15] Rasolofosaon PNJ. Importance of interface hydraulic condition on the generation of second bulk compressional wave in porous media. *Applied Physics Letters* 1988;52:780–2.
- [16] Yang J, Sato T. Seismic response of a partially saturated sand layer. In: Proceedings of the 10th Japan Earthquake Engineering Symposium, Yokohama, 1998. p. 799–804.
- [17] Stoll RD. *Sediment acoustics*. Berlin: Springer-Verlag: lecture notes in earth sciences, 1989.
- [18] Jonson DL, Kopic J, Dashen R. Theory of dynamic permeability and tortuosity in fluid saturated porous media. *Journal of Fluid Mechanics* 1987;176:379–402.
- [19] Richart FE, Hall JR, Woods RD. *Vibrations of soils and foundations*. NJ: Prentice Hall, 1970.